Published in final edited form as:
J Nucl Med. 2011 February ; 52(2): 225–230. doi:10.2967/jnumed.110.083162.

Assessment of Tumoricidal Efficacy and Response to Treatment with ^{18}F-FDG PET/CT After Intraarterial Infusion with the Antiglycolytic Agent 3-Bromopyruvate in the VX2 Model of Liver Tumor

Eleni Liapi[1], **Jean-Francois H. Geschwind**[1], **Mustafa Vali**[1], **Afsheen A. Khwaja**[1], **Veronica Prieto-Ventura**[1], **Manon Buijs**[1], **Josephina A. Vossen**[1], **Shanmugasudaram Ganapathy**[1], and **Richard L. Wahl**[2]

[1]Division of Interventional Radiology, Russell H. Morgan Department of Radiology and Radiological Sciences, Johns Hopkins University, Baltimore, Maryland [2]Division of Nuclear Medicine, Russell H. Morgan Department of Radiology and Radiological Sciences, Johns Hopkins University, Baltimore, Maryland

Abstract

The purpose of this study was to determine the effects of 3-bromopyruvate (3-BrPA) on tumor glucose metabolism as imaged with ^{18}F-FDG PET/CT at multiple time points after treatment and compare them with those after intraarterial control injections of saline.

Methods—Twenty-three New Zealand White rabbits implanted intrahepatically with VX2 tumors were assigned to 1 of 2 groups: 14 rabbits were assigned to the treatment group (TG) and 9 to the saline control group (SG). All animals were infused with 25 mL of either 1.75 mM 3-BrPA or saline over 1 h via a 2-French catheter, which was secured in the hepatic artery. For PET/CT, the animals were injected with 37 MBq of ^{18}F-FDG at 1 d before treatment and 2 h, 24 h, and 1 wk after treatment. Tumor size, tumor and liver maximal standardized uptake value (SUV_{max}), and tumor-to-background ratios were calculated for all studies. Seven TG and 5 SG animals were sacrificed at 1 wk after treatment for histopathologic analysis.

Results—Intense ^{18}F-FDG uptake was seen in untreated tumors. A significant reduction in tumor SUV_{max} was noted in TG animals, when compared with SG animals, at 1 wk after treatment ($P = 0.006$). The tumor–to–liver background ratio in the TG animals, compared with the SG animals, was significantly reduced as early as 24 h after treatment ($P = 0.01$) and remained reduced at 1 wk ($P = 0.003$). Tumor SUV_{max} increased from the baseline levels at 7 d in controls ($P = 0.05$). The histopathologic analysis of explanted livers revealed increased tumor necrosis in all TG samples. There was a significant inverse correlation ($r^2 = 0.538$, $P = 0.005$) between the

For correspondence or reprints contact either of the following: Richard L. Wahl, Division of Nuclear Medicine, Russell H. Morgan Department of Radiology and Radiological Sciences, Johns Hopkins Medical Institutions, 601 N. Caroline St., Rm. 3223A, Baltimore, MD 21287-0817. rwahl@jhmi.edu. Jean-Francois Geschwind, Johns Hopkins University School of Medicine, 600 N. Wolfe St., Blalock 545, Baltimore, MD 21287. jfg@jhmi.edu.

percentage of tumor necrosis on histopathology and tumor SUV_{max} on ^{18}F-FDG PET at 7 d after treatment with 3-BrPA.

Conclusion—Intraarterial injection of 3-BrPA resulted in markedly decreased ^{18}F-FDG uptake as imaged by PET/CT and increased tumor necrosis on histopathology at 1 wk after treatment in the VX2 rabbit liver tumor. PET/CT appears to be a useful means to follow antiglycolytic therapy with 3-BrPA.

Keywords

hepatology; PET/CT; 3-bromopyruvate; VX2; interventional; liver cancer

The fundamental knowledge that cancer cells frequently exhibit enhanced glycolysis to meet their energy needs, even under aerobic conditions, is known as the Warburg effect (1,2). Although the underlying and regulatory mechanisms responsible for this effect are complicated and not yet fully explored, the metabolic consequences appear to be similar; cancer cells shift their means of energy production toward increased glycolysis for adaptation and survival (3,4).

^{18}F-FDG PET traces the tissue concentrations of ^{18}F, which are directly related to the glucose metabolic rate, as most intratumoral ^{18}F is in the form of FDG-6-phosphate and is thus a noninvasive indicator of the Warburg phenomenon and of tumor glucose use (5). ^{18}F-FDG is a glucose analog that is preferentially trapped in fast-metabolizing cells, such as cancer cells, in the form of FDG-6-phosphate. Increased ^{18}F-FDG uptake has been noted in many types of tumor xenografts (6). In recent years, ^{18}F-FDG PET has become increasingly important in cancer management and is now routinely used in the diagnosis and staging of many malignancies as well as in the evaluation of the response to treatment (7).

Not surprisingly, the Warburg effect also provides an important biochemical basis for the design of anticancer therapeutic strategies and new anticancer agents. 3-bromo-pyruvate (3-BrPA) belongs to a new class of anticancer drugs blocking glycolytic tumor metabolism and has shown promising results when injected intraarterially in the VX2 tumor model of liver cancer (8,9). In this report, we used the VX2 liver tumor model to determine the tumoricidal effects of 3-BrPA over time and monitor changes in tumor metabolism and tumor response to treatment with ^{18}F-FDG PET. We have previously shown that this moderate-sized rabbit tumor model is well imaged using modern clinical PET/CT capabilities (10). We further sought to determine whether metabolic imaging response to treatment correlates with histopathologic tumor necrosis.

MATERIALS AND METHODS

This study was approved by our institution’s Animal Care and Use Committee, and experiments were performed according to its guidelines. Twenty-three New Zealand White male rabbits (Myrtle Rabbits), weighing 3.5–4.2 kg, were used for this study and were assigned to 1 of 2 groups. Fourteen rabbits were assigned to the treatment group (TG), and 9 were assigned to the saline control group (SG).

Tumor Implantation

A suspension (0.4 mL) containing approximately 1×10^6 VX2 tumor cells (derived from a tumor carrier rabbit) was first injected into the thigh muscles of a carrier rabbit and maintained for 14 d for adequate tumor growth. Each intramuscularly developed VX2 tumor was removed under general anesthesia, minced to 1-mm pieces, and placed in Hank's solution. Each carrier rabbit was used to supply tumor pieces for implantation into the left lobe of the liver of 5 separate rabbits. Anesthesia was induced in all of the animals with a mixture of acepromazine (2.5 mg/kg) and ketamine hydrochloride (44 mg/kg) administered intramuscularly and maintained by intravenous injection of sodium pentothal via a marginal ear vein. Then, the abdomens of the recipient rabbits were shaved and prepared with povidone-iodine surgical scrub solution, after which a midline subxiphoid incision was made. The anterior surface of the liver was exposed, and tumor pieces (0.1–0.2 mL) from the minced donor tumor were directly implanted into the left lobe of the liver using the outer cannula of a 21-gauge angiocatheter. This method typically allows the growth of 1 well-demarcated tumor in the liver of each recipient rabbit. The abdomen was closed in 2 layers. Proper aseptic technique was rigorously observed during each implantation. After surgery, animals were returned to their cages, kept warm with blankets, and monitored until they recovered from anesthesia. Buprenorphine (0.01 mg) was administered postoperatively in all animals for pain control. The tumors were allowed to grow for 14 d, at which time they had typically reached a well-demarcated spheric shape, with the largest diameter ranging from 1.5 to 2.0 cm (tumors were not visible from outside the body).

Preparation of 3-BrPA Solutions

After adjusting the pH to 7.0 with $NaHCO_3$, the 3-BrPA solutions (Sigma Chemical) were prepared in phosphate-buffered saline, sterilized with a 0.22-μm filter unit (Millex GV; Millipore), and used immediately.

Transcatheter Intraarterial Infusions

Anesthesia was induced and maintained as described in the "Tumor Implantation" section. Transcatheter hepatic artery injections of either 3-BrPA or saline were performed under fluoroscopic guidance. The animals were brought to the angiography suite and intubated using a 3.0-mm endotracheal tube (Mallinkrodt Medical) to monitor respiration rate and end-tidal CO_2. Access to the right femoral artery was obtained via surgical cut-down and insertion of a 3-French sheath (Cook). A specially manufactured 2-French catheter with a tip in the shape of a hockey stick (JB1 catheter; Cook) was then advanced inside the aortic lumen and into the celiac axis. Then, a celiac arteriogram was obtained to delineate the blood supply to the liver and confirm the location of the tumor. The tumor could readily be visualized as a hypervascular round area on the left side of the liver near the gastric fundus. The left hepatic artery was then selectively catheterized via the common hepatic artery using a steerable guidewire (Transcend wire, 0.035 cm [0.014 in]; Boston Scientific). After the catheter was adequately positioned within the left hepatic artery, the 3-BrPA solution (or saline control) was then infused directly into the artery with a previously standardized method (9). A syringe containing 25 mL of 3-BrPA (1.75 mmol/L) or 25 mL of 0.9% NaCl was connected to the end of the JB1 catheter and carefully placed and adjusted on an

infusion syringe pump (Harvard Apparatus model 11 infuse/withdraw single-syringe pump; Instech Solomon). The injection rate was set at 25 mL per hour. During the 1-h infusion, maintenance of appropriate positioning of the catheter in the hepatic artery was monitored with fluoroscopy. All animals were monitored after the procedure and given analgesics postoperatively.

^{18}F-FDG PET/CT Protocol

^{18}F-FDG PET/CT was performed at 24 h before treatment (baseline) and 2 h, 24 h, and 1 wk after treatment, in a combined clinical PET/4-slice CT scanner (Discovery LS; GE Healthcare). After at least 4 h of fasting, about 37 MBq (1 mCi) of ^{18}F-FDG were administered intravenously to each rabbit via a marginal ear vein and under anesthesia. Fifty minutes later, 4-section unenhanced spiral CT covering the thorax and abdomen was performed. The imaging parameters used in this study had been previously reported (10). The technical parameters used for the unenhanced CT portion of PET/CT were as follows: a detector row configuration of 4 × 5 mm; pitch of 6:1 (high-speed mode); voltage of 120 kVp; current of 80 mA; large scan field of view (FOV); and display FOV of 50 cm. The unenhanced CT scan was used for attenuation correction and for automatic image fusion.

CT images were reconstructed into 5-mm-thick sections at 4.25-mm intervals and subsequently used to correct the PET emission images for attenuation. A whole-body emission PET scan for the same axial coverage was obtained in the 2-dimensional acquisition mode with 5 min of acquisition per bed position and a total of 2 PET bed positions. A high-resolution contrast-enhanced CT image was then acquired, using the following parameters: a detector row configuration of 4 × 1.25 mm; pitch of 3:1 (high-quality mode); voltage of 120 kVp; current of 120; large scan FOV; display FOV of 35 cm; and scan delay of 10 s. Contrast (Omnipaque 350; Nycomed) was injected in all rabbits (5-mL dose via marginal ear vein) after PET. The animals were kept under anesthesia from the time of ^{18}F-FDG injection until the end of imaging. The 5-mm-thick/4.25-mm-interval transaxial CT images of 50-cm FOV were reconstructed for automatic fusion with 50-cm-FOV PET images. ^{18}F-FDG PET, CT, and 50-cm-FOV fused ^{18}F-FDG PET/CT images were generated on a computer workstation, using vendor-supplied software (Xeleris; GE Healthcare). Glucose blood levels were measured before and after each scan.

PET/CT Data Analysis

For quantitative analysis of the acquired ^{18}F-FDG PET images, loosely fit regions of interest covering the whole tumor were placed manually over every axial image plane in which tumor tissue was visualized as abnormally increased ^{18}F-FDG accumulation. Tumor maximal standardized uptake values (SUV_{max}) were obtained on multiple planes for each rabbit, and the highest SUV_{max} was then recorded for both tumor and liver parenchyma. In a similar fashion, 1-cm circular regions of interest were drawn over the left and right liver over every axial image plane where the hepatic parenchyma could be visualized, and the SUV_{max} was then chosen. Tumor–to–liver background (T/L) ratios were calculated for all studies by dividing the tumor SUV_{max} by the contralateral hepatic parenchymal SUV_{max}. CT measurements included maximal bidimensional tumor size diameters, as recorded on the contrast-enhanced CT scan.

Histopathology

Seven TG and 5 SG animals were sacrificed at 1 wk after treatment for histopathologic analysis. The remaining animals were included in a subsequent survival analysis study (11). Liver tissues and tumors were fixed in 10% formalin, sliced at 5-mm intervals for gross examination, and then embedded completely in paraffin. Each slide of the 4-μm-thick sections per sample was then stained with hematoxylin and eosin. Tumor necrosis was evaluated by a postdoctoral fellow, specifically trained to perform this task with the assistance of a tumor biologist, using digital image analysis for accurate quantification. The center image of the completely embedded tumor was digitized using a digital camera (Axiovert 200; Zeiss) attached to a microscope with high-quality optical lenses. Each tumor image was then imported into Image J (National Institutes of Heath; http://rsb.info.nih.gov/ij/) for quantification of tumor necrosis. The tumor was divided into 4 quadrants (2 fields per quadrant). For each quadrant, the margin of the tumor and the area of necrosis were outlined. Subsequently, the software program determined the surface areas of the tumor and necrotic portion. The percentage of tumor necrosis was then calculated for each quadrant (local percentage necrosis) and for the entire tumor (global percentage necrosis).

Statistical Analysis

Statistical analysis included descriptive data for all tested parameters, *t* tests between different treatment variables for each time point, and intragroup comparisons with a *P* value of less than 0.05. Correlation coefficients were also calculated to measure strength of association between tumor SUV_{max} and percentage of necrosis on histopathology. ANOVA was used to compare data over time and among groups. STATA 9 statistical software was applied (StataCorp LP).

RESULTS

All animals had hypervascular tumors on angiography and were subsequently successfully treated (Fig. 1). No peri-or postprocedural complications were observed. Tumors were ^{18}F-FDG–avid before treatment, with a mean baseline SUV_{max} ± SD of 6.1 ± 2.42 in the TG and 6.06 ± 2.75 in the SG ($P = 0.51$). At 2 h, 24 h, and 1 wk after treatment, when compared with baseline values, ^{18}F-FDG tumor uptake in the TG showed a statistically significant change (at 2 h, $P = 0.009$; 24 h, $P = 0.0005$; and 1 wk, $P = 0.01$). At 1 wk after treatment, there was a statistically significant decrease in^{18}F-FDG tumor uptake in the TG (SUV_{max}, 4.18 ± 1.36) compared with the SG (SUV_{max}, 9.0 ± 3.17) ($P = 0.006$).

The T/L ratios confirmed that at 2 h there was significantly decreased ^{18}F-FDG T/L uptake, when compared with baseline values in the TG ($P = 0.005$). The comparison of TG and SG T/L ratios showed a statistically significant difference at 24 h after treatment ($P = 0.01$). At 1 wk after treatment, the T/L ratio of the TG, compared with the SG, significantly decreased (1.56 ± 0.71 vs. 3.47 ± 0.10; $P = 0.003$; Figs. 2A and 2B; Table 1). No statistically significant changes in tumor maximal axial diameters were seen over time between the 2 groups (Table 1). Interestingly, there was a slight increase in tumor size of the TG animals at 2 h after treatment, when compared with their starting baseline axial tumor diameters (Table 1).

A statistically significant difference in tumor SUV_{max} and T/L ratio with time (repeated-measures ANOVA, $P = 0.04$ and $P = 0.03$, respectively) was observed in the SG. No significant difference in SUV_{max} with time (repeated-measures ANOVA, $P = 0.06$) was observed in the TG, whereas there was a significant difference in T/L ratio with time (repeated-measures ANOVA, $P = 0.0007$). The differences that were identified in the SG for both SUV_{max} and T/L ratio indicate intragroup increased variability, whereas the SUV_{max} measurements in the TG were more reproducible over time.

On histopathology, mean tumor necrosis in the TG at 7 d was 89.8% ± 1.9%, with minimal liver fatty changes and liver necrosis, whereas mean tumor necrosis in the SG was 34.16% ± 3.7% (Figs. 3A and 3B). There was a significant inverse correlation between the percentage of necrosis on histopathology and the tumor SUV_{max} at 1 wk after treatment ($r^2 = -0.573$, $P = 0.005$, Fig. 4).

DISCUSSION

Although some biochemical properties of 3-BrPA as an effective inhibitor of enzymes were reported more than 2 decades ago, it was only recently that its potential as an antiglycolytic and anticancer agent was recognized (8,12,13). Several routes of 3-BrPA delivery have been tested, to identify optimal drug uptake by the tumor with minimal side effects (9). A previous report determined that a highly effective route of drug delivery was via the arteries that feed the tumor and that a highly effective intra-arterial dose frequently causing complete tumor death without causing any overt toxicity to nontumorous normal liver tissue was 1.75 mM of 3-BrPA in 25 mL of phosphate-buffered saline infused over a period of 1 h in a rabbit model system (9). This dose regimen was based on the combination of efficacy (tumor kill) and toxicity determined histopathologically (9). From a therapeutic intervention perspective, locoregional drug delivery may have superiority over systemic chemotherapy because the non-specific toxicity of remote nontargeted cells is minimized or avoided.

Because 3-BrPA treatment inhibits tumor cell metabolism and glucose uptake, PET/CT, using ^{18}F-FDG, a radioactive analog of glucose, would be expected to be a highly appropriate method for assessing tumor response to therapy. Our results showed that tumors treated with 3-BrPA showed a statistically significant decrease ^{18}F-FDG uptake as early as 2 h after treatment. Interestingly, a slight decrease (not statistically significant) in tumor ^{18}F-FDG uptake was also noted in the SG at 2 h after treatment, presumably attributed to catheter manipulations, which likely lead to vessel spasm, interruption of arterial blood flow to the tumor, and reduced ^{18}F-FDG input to the tumor. An instant drop in ^{18}F-FDG uptake has been seen immediately after transcatheter arterial embolization (14). A slight increase in tumor size was seen at 2 h after infusion, which may be due to increased fluid retention. A similar phenomenon has been observed after intraarterial chemoembolization in patients with unresectable hepatocellular carcinoma (15).

We assessed both SUV_{max} and T/L ratios. A similar approach with reference to the liver has been suggested in the recent PET Response Criteria in Solid Tumors (16). The T/L ratio confirmed changes in the effect of treatment earlier than $SUV_{max,}$ indicating that this ratio may be a more sensitive marker than SUV_{max} for detecting early functional changes. Both

T/L ratio and SUV_{max} demonstrated statistically significant differences between TG and SG at 1 wk after treatment, suggesting that the tumoricidal efficacy of 3-BrPA is sustained.

Histopathologic analysis at 1 wk showing increased tumor cell death correlates significantly with the ^{18}F-FDG PET/CT findings. It is therefore apparent that 3-BrPA may effectively target the VX2 tumors and that ^{18}F-FDG PET is a valuable method of monitoring tumor glucose metabolism changes in response to treatment with 3-BrPA. Several studies have shown that changes in tumor metabolism occur early in the course of chemotherapy and precede the reduction of tumor size (17–19). No tumor size reduction was noted during the time interval for our study experiment. In fact, there was a slight increase in tumor size over time, as could be attributed to the aggressive nature of the VX2 tumor model (20). The time interval of 7 d may also be inadequately short to detect possible changes in tumor size after treatment. Further, the large fraction of necrosis in the TG with no major change in tumor diameter reflects the limitations of anatomic imaging alone in assessing response soon after treatments are started.

Our study had several limitations. Not all animals had their tumors available and assessed histologically. Further, whereas SUV_{max} and T/L ratios were used, it is possible more accurate quantitative results could have been obtained using dynamic data acquisitions. Such analyses might have been able to separate the delivery from the phosphorylation events in the analysis. However, it may be argued that dynamic PET protocols are less suitable for routine clinical application because of the longer scanning times and the necessity of arterial blood sampling, which can be too much of a burden to the patient. We therefore chose a protocol that can easily be transferred to the clinic and reproduced in many institutions.

All animals in our study were anesthetized during imaging. Previous studies on the effect of anesthetics on glucose metabolism have shown that ketamine dose-dependently affects rabbit plasma glucose. Low doses (1–2 mg/kg) of ketamine produce hyperglycemia, whereas higher doses (2 mg/kg) produce hypoglycemia. However, at the dose level of 4 mg/kg, there is no effect on blood glucose levels. Pentothal is metabolized by the liver and can affect liver function (increase in liver enzymes). The effect of the anesthetics should be negligible, however, because all rabbits received comparable levels of preanesthetic and anesthetic drugs and doses.

Further histopathologic confirmation of our ^{18}F-FDG PET/CT data is needed on a larger sample of animals sacrificed at different time points. Further development and studies of this glycolytic inhibitor are necessary to establish its clinical therapeutic safety and efficacy and possible extension to human studies. Nonetheless, the major and significant declines in tumor glycolysis shortly after treatment is begun are indicators of a substantial and important biologic effect of this therapy and further support its mechanism of action.

CONCLUSION

An intraarterial injection of 3-BrPA resulted in markedly decreased ^{18}F-FDG uptake as assessed by ^{18}F-FDG PET/CT, effects on metabolism much greater than on tumor size, and effective tumor kill in the VX2 animal model of liver cancer. On histopathology, at 1 wk

after treatment, significant tumor necrosis was demonstrated in all treated tumor samples, strongly inversely correlating with decreased tumor SUV_{max}. These preliminary studies confirm the potential of 3-BrPA as an effective treatment for liver cancer and the utility of ^{18}F-FDG PET/CT for both tracking delivery of functionally relevant 3-BrPA to the target tumor and monitoring the effects of therapy over time.

Acknowledgments

This study was supported by NIH/NCI grant RO1 CA100882-01 and the T32 grant 5T32EB006351-02.

References

1. Warburg O. On the origin of cancer cells. Science. 1956; 123:309–314. [PubMed: 13298683]
2. Kroemer G, Pouyssegur J. Tumor cell metabolism: cancer's Achilles' heel. Cancer Cell. 2008; 13:472–482. [PubMed: 18538731]
3. Pelicano H, Martin DS, Xu RH, Huang P. Glycolysis inhibition for anticancer treatment. Oncogene. 2006; 25:4633–4646. [PubMed: 16892078]
4. Kondoh H. Cellular life span and the Warburg effect. Exp Cell Res. 2008; 314:1923–1928. [PubMed: 18410925]
5. Kelloff GJ, Hoffman JM, Johnson B, et al. Progress and promise of FDG-PET imaging for cancer patient management and oncologic drug development. Clin Cancer Res. 2005; 11:2785–2808. [PubMed: 15837727]
6. Wahl RL, Hutchins GD, Buchsbaum DJ, Liebert M, Grossman HB, Fisher S. ^{18}F-2-deoxy-2-fluoro-D-glucose uptake into human tumor xenografts: feasibility studies for cancer imaging with positron-emission tomography. Cancer. 1991; 67:1544–1550. [PubMed: 2001543]
7. Avril NE, Weber WA. Monitoring response to treatment in patients utilizing PET. Radiol Clin North Am. 2005; 43:189–204. [PubMed: 15693656]
8. Geschwind J-FH, Ko YH, Torbenson MS, Magee C, Pedersen PL. Novel therapy for liver cancer: direct intraarterial injection of a potent inhibitor of ATP production. Cancer Res. 2002; 62:3909–3913. [PubMed: 12124317]
9. Vali M, Liapi E, Kowalski J, et al. Intraarterial therapy with a new potent inhibitor of tumor metabolism (3-bromopyruvate): identification of therapeutic dose and method of injection in an animal model of liver cancer. J Vasc Interv Radiol. 2007; 18:95–101. [PubMed: 17296709]
10. Tatsumi M, Nakamoto Y, Traughber B, Marshall LT, Geschwind JF, Wahl RL. Initial experience in small animal tumor imaging with a clinical positron emission tomography/computed tomography scanner using 2-[F-18]fluoro-2-deoxy-D-glucose. Cancer Res. 2003; 63:6252–6257. [PubMed: 14559811]
11. Vali M, Vossen JA, Buijs M, et al. Targeting of VX2 rabbit liver tumor by selective delivery of 3-bromopyruvate: a biodistribution and survival study. J Pharmacol Exp Ther. 2008; 327:32–37. [PubMed: 18591216]
12. Geschwind JF, Georgiades CS, Ko YH, Pedersen PL. Recently elucidated energy catabolism pathways provide opportunities for novel treatments in hepatocellular carcinoma. Expert Rev Anticancer Ther. 2004; 4:449–457. [PubMed: 15161443]
13. Xu, R-h; Pelicano, H.; Zhou, Y., et al. Inhibition of glycolysis in cancer cells: a novel strategy to overcome drug resistance associated with mitochondrial respiratory defect and hypoxia. Cancer Res. 2005; 65:613–621. [PubMed: 15695406]
14. Oya N, Nagata Y, Tamaki N, et al. FDG-PET evaluation of therapeutic effects on VX2 liver tumor. J Nucl Med. 1996; 37:296–302. [PubMed: 8667065]
15. Kamel IR, Liapi E, Reyes DK, Zahurak M, Bluemke DA, Geschwind JF. Unresectable hepatocellular carcinoma: serial early vascular and cellular changes after transarterial chemoembolization as detected with MR imaging. Radiology. 2009; 250:466–473. [PubMed: 19188315]

16. Wahl RL, Jacene H, Kasamon Y, Lodge MA. From RECIST to PERCIST: evolving considerations for PET response criteria in solid tumors. J Nucl Med. 2009; 50(suppl 1):122S–150S. [PubMed: 19403881]

17. Ott K, Fink U, Becker K, et al. Prediction of response to preoperative chemotherapy in gastric carcinoma by metabolic imaging: results of a prospective trial. J Clin Oncol. 2003; 21:4604–4610. [PubMed: 14673049]

18. Avril N, Sassen S, Schmalfeldt B, et al. Prediction of response to neoadjuvant chemotherapy by sequential F-18-fluorodeoxyglucose positron emission tomography in patients with advanced-stage ovarian cancer. J Clin Oncol. 2005; 23:7445–7453. [PubMed: 16157939]

19. Wahl RL, Zasadny K, Helvie M, Hutchins GD, Weber B, Cody R. Metabolic monitoring of breast cancer chemohormonotherapy using positron emission tomography: initial evaluation. J Clin Oncol. 1993; 11:2101–2111. [PubMed: 8229124]

20. Boehm T, Malich A, Goldberg SN, et al. Radio-frequency tumor ablation: internally cooled electrode versus saline-enhanced technique in an aggressive rabbit tumor model. Radiology. 2002; 222:805–813. [PubMed: 11867805]

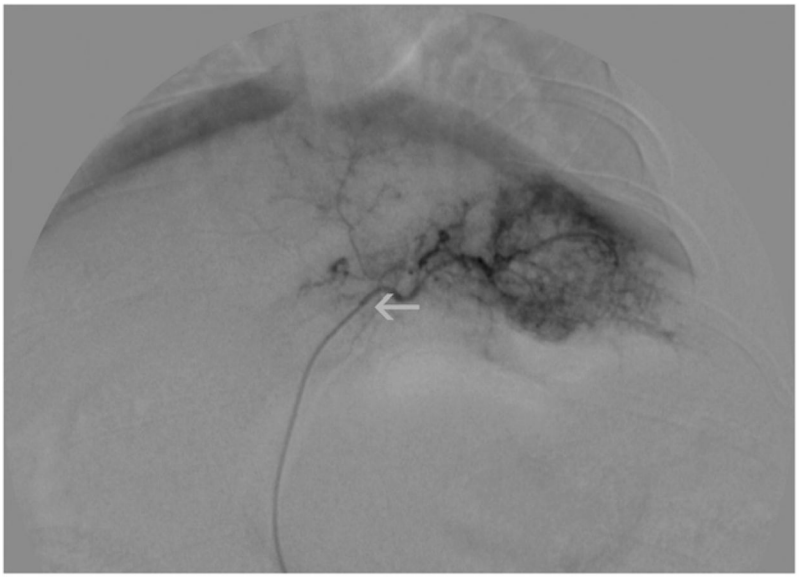

FIGURE 1.

Digital subtraction angiographic view of VX2 tumor in liver before treatment. Tumor is hypervascular. Catheter is inside tumor's feeding artery, close to tumor (superselective catheterization, white arrow).

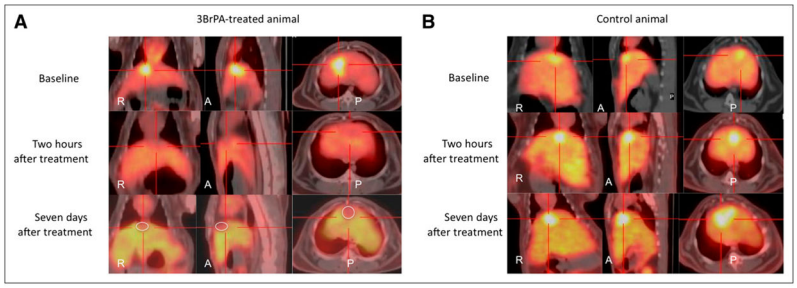

FIGURE 2.

(A) Fused ^{18}F-FDG PET/CT images (axial, coronal, and sagittal views) of VX2 liver tumor at 24 h before treatment with 3-BrPA, 2 h after treatment, and 1 wk after treatment. Tumor ^{18}F-FDG uptake progressively decreases over time, and central necrosis develops in tumor after treatment (circle). (B) Fused ^{18}F-FDG PET/CT images (axial, coronal, and sagittal views) of VX2 liver tumor at 24 h before treatment with saline, 2 h after treatment, and 1 wk after treatment. Tumor ^{18}F-FDG uptake progressively increases over time. A = anterior; P = posterior.

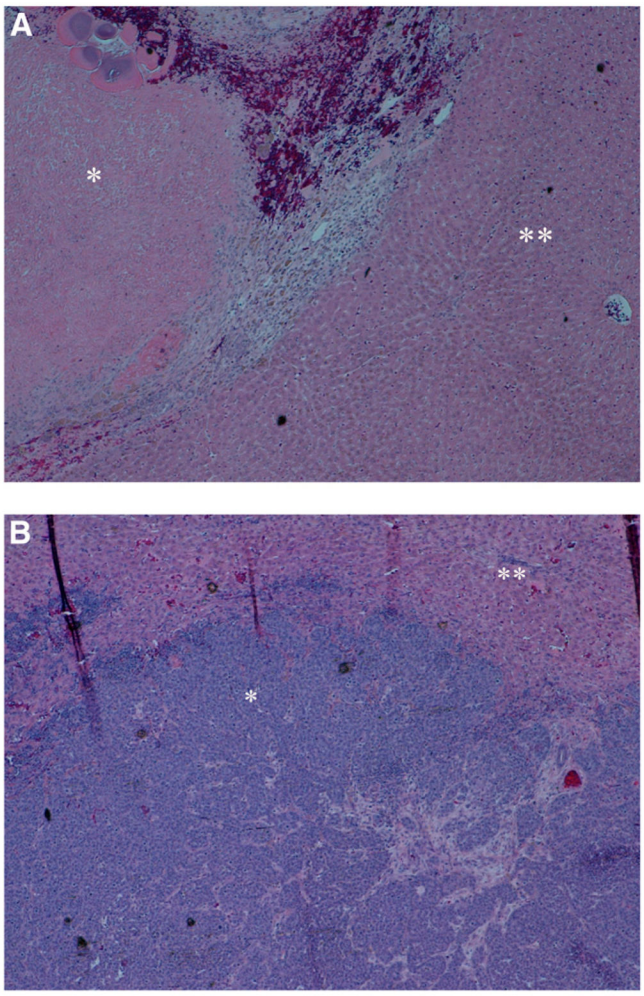

FIGURE 3.

Histopathologic images of tumors, stained with hematoxylin and eosin. (A) Representative image of treated tumor, at level of tumor periphery, surrounded by normal hepatic parenchyma. There is increased tumor necrosis. (B) Representative image of untreated tumor, again at level of tumor periphery, surrounded by normal hepatic parenchyma. * = tumor; ** = hepatic parenchyma.

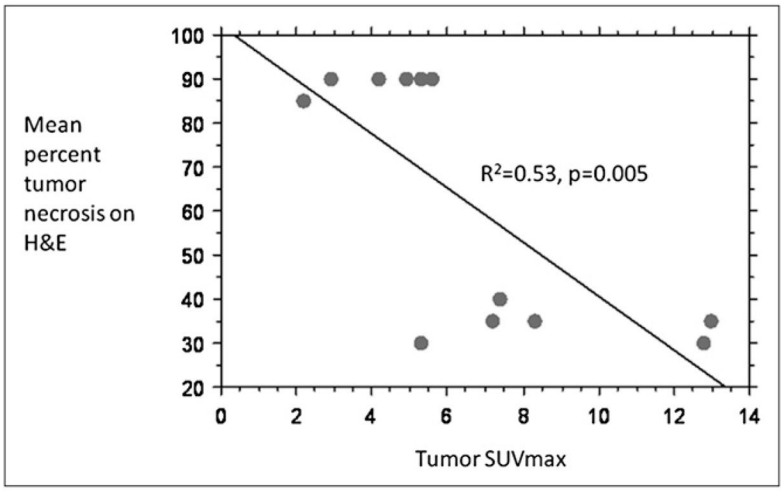

FIGURE 4.

Bivariate scattergram showing correlation between mean percentage tumor necrosis (hematoxylin and eosin) and tumor SUV_{max} at 7 d for all groups (TG and SG). H&E = hematoxylin and eosin.

TABLE 1

^{18}F-FDG Tumor SUV_{max}, T/L Ratio, and Tumor Maximal Axial Diameter Values in TGs and SGs

		Tumor ^{18}F-FDG uptake SUV_{max}				Tumor-to-liver ratio				Tumor maximal axial diameter (cm)				
Study time point	**Animal group**	**Mean**	**SD**	***P* value 1**	***P* value 2**	**Mean**	**SD**	***P* value 1**	***P* value 2**	**Mean**	**SD**	***P* value 1**	***P* value 2**	**Normal liver SUV_{max}**
Baseline	TG	6.10	2.42			2.49	0.81			1.91	0.71			2.49
	SG	6.06	2.75	0.51		2.70	1.26	0.67		2.27	0.85	0.88		2.34
After treatment														
2 h	TG	3.32	3.17		0.009	1.4	0.7		0.005	2.45	0.49		0.98	2.19
	SG	4.61	1.47	0.12	0.87	1.89	0.52	0.09	0.91	2.56	0.83	0.38	0.26	2.57
24 h	TG	3.06	0.87		0.0005	1.17	0.33		0.002	2.58	0.67		0.96	3.33
	SG	5.30	2.00	0.09	0.67	1.72	0.21	0.01	0.95	2.66	0.56	0.42	0.20	3.10
1 wk	TG	4.18	1.36		0.01	1.56	0.71		0.02	2.76	0.72		0.01	2.97
	SG	9.00	3.17	0.006	0.05	3.47	1.1	0.003	0.13	3.05	0.84	0.27	0.05	2.93

Intergroup comparisons (*P* value 1) and intragroup comparisons (*P* value 2, comparison to baseline values) were made using mean values for each variable, and $P < 0.05$ indicates statistically significant differences between groups. *P* values refer to unpaired *t* tests with unequal variance. Reference SUV_{max} of normal hepatic parenchyma are also included.

J Nucl Med. Author manuscript; available in PMC 2015 February 23.